DOI: 10.1002/chem.200500992

Fine-Tuning of Relative Metal–Metal Distances within Highly Ordered Chiral 2D Nanopatterns

Philipp Zell,[a] Florian Mögele,[a] Ulrich Ziener,[b] and Bernhard Rieger*[a]

Abstract: The two-dimensional nanopatterning of a series of neutral alkoxy/alkyl-functionalised bis(salicylaldehydato)/bis(aldiminato)copper(II) and -palladium(II) complexes at a liquid/solid (highly oriented pyrolytic graphite, HOPG) interface has been studied by scanning tunnelling microscopy (STM). The relative metal–metal distances were tuned stepwise in two dimensions by ligand design. Exchange of the carbonyl O-atom for NH or *N*-alkyl units effects different intermolecular interactions such as weak hydrogen bonds and steric effects that determine, together with the van der Waals forces between the alkyl chains, the relative arrangements of the complexes. Further variation of the length and position of the alkoxy side chains as well as the exchange of Cu^{II} for Pd^{II} affords an absolute fine-tuning of the surface structures. Highly resolved STM images of the resultant highly ordered adlayers allow us to establish detailed models of the molecular 2D arrays and to classify them into three basic chiral pattern types. Homochirality within the individual domains is induced by the highly regular deposition of the prochiral complexes from the same enantiotopic face. In the case of the C_{12} O-substituted bis(salicylaldiminato) (NH) Cu^{II} complex **Cu5**, a secondary structure occurs as a racemic mixture of two chiral surface species deposited in a distinct alternating order.

Keywords: chirality · metal complexes · nanostructures · scanning probe microscopy · self-assembly

Introduction

The preparation of highly ordered nanostructures by self-assembly of defined metal complexes on solid surfaces is a field of growing interest.[1–4] In analogy to the common practices applied for organic compounds, techniques such as vapour deposition[3,5,6] and the preparation of Langmuir–Blodgett (LB) films[7] have been used to form adlayers of metal complexes that can be visualised by scanning tunnelling microscopy (STM). A further effective method for the formation of monolayers is self-assembly at liquid/solid interfaces, which typically results in highly ordered and widely extended surface layers. This method provides the best choice for compounds that do not tolerate vaporisation due to thermal decomposition, as is often observed for metal complexes. As a further advantage amphiphilic properties, as in the case of the LB technique, are not required. In contrast, alkyl side chains often serve as anchor groups that promote the recognition and stabilisation of individual molecules at the liquid/solid interface.[8–12] Following this strategy metal ions can be incorporated into the surface layers either by complexation in situ with organic template structures that contain suitable binding sites for metal complexation, or by direct deposition of isolated metal complexes. De Feyter and co-workers, for example, have observed an in situ complexation of Pd^{2+} and Cu^{2+} ions in bipyridine-derived 2D matrices by the characteristic changes of their molecular order.[13,14] In a similar way, Qian et al. have achieved the complexation of Cu^{2+} ions to *n*-octadecylsalicylaldimine adlayers.[15] A more common approach—the direct 2D self-assembly of well-defined metal complexes—has been exploited in the field of phthalocyanine and porphyrin complexes, where the alkyl side chains determine the distances between the individual metal centres.[16,17] Besides these macrocyclic complexes, Ni^{II}–salen[18] and Cu^{II}–dionato complexes[19] bearing alkyl functionalities have been visualised

[a] P. Zell, F. Mögele, Prof. Dr. B. Rieger
Department of Materials and Catalysis
University of Ulm
Albert-Einstein-Allee 11, 89081 Ulm (Germany)
Fax: (+49) 731-502-3039
E-mail: Bernhard.Rieger@uni-ulm.de

[b] Dr. U. Ziener
Department of Organic Chemistry III
University of Ulm
Albert-Einstein-Allee 11, 89081 Ulm (Germany)

Supporting information for this article is available on the WWW under http://www.chemeurj.org/ or from the author.

at a liquid/solid interface. More recently, Gong et al. have reported the self-assembly of a supramolecular, tetranuclear rectangle[20] where the resultant 2D arrays depend significantly on the substrate used.

One important goal in this field is the generation of functional surfaces. Our studies focus on fundamental approaches to an easy variation of relative metal–metal distances, which is the basis for the fine-tuning of specific surface features. The resultant nanopatterned surfaces could be interesting for application as catalysts, sensors or as programmable matrices or building blocks for the "bottom-up" engineering of electronic or magnetic devices. In addition to the high regularity of the defined nanostructures, self-assembled monolayers often exhibit local 2D chirality, and chiral monolayers can be formed on planar surfaces from both chiral and achiral compounds.[21,22] In the latter case, chirality is induced either by the highly regular face-on deposition of prochiral compounds onto a substrate[22–27] or by the specific 2D packing of non-prochiral molecules.[23,28,29] It should be mentioned, of course, that the 2D adsorption of prochiral molecules can also lead to overall achiral (racemic) 2D structures depending on the specific packing pattern (see below).

Recently, we have reported that salicylaldehyde- and -aldimine-derived Cu^{II} complexes form different 2D structures at a solution/HOPG interface, as determined by STM.[30] We have now applied these findings as a basic concept for the generation of monolayers with fine-tuned nanostructures by exploiting the effects of variation of the functional groups as well as exchange of the metal ions on the 2D packing. Furthermore, we have extended the previous structure models[30] and established basic homochiral pattern types for the observed 2D arrays.

Results and Discussion

Synthesis of alkyl/alkoxy-substituted bis-salicylaldehydato/-aldiminato–M^{II} complexes: Prior to the STM investigations, a series of neutral salicylaldehyde- and -aldimine-derived M^{II} complexes with variable position and length of the alkoxy substituents (Y) as well as exchangeable functional groups (X) was synthesised and fully characterised (Scheme 1, Table 1). The free 4-alkoxy-substituted salicylaldehydes **Sa1**–**Sa3** were obtained following general methodologies previously reported in the literature, namely by selective etherification of the 4-hydroxysalicylaldehyde precursor with *n*-alkyl bromides in the presence of K_2CO_3 in DMF.[31,32] The analogous 5-substituted compound **Sa4** was accessible by the incorporation of a formyl group into an alkoxyphenol synthon[33] by reaction with hexamethylenetetramine in refluxing trifluoroacetic acid.[34] The desired M^{II} complexes were obtained subsequently in one further step: The alkoxy-substituted bis(salicylaldehydato)copper(II) and -palladium(II) complexes **Cu1**, **Cu2**, **Pd1** and **Pd2** were synthesised by treatment of the free salicylaldehyde-derived ligands **Sa** with the M^{II} acetate precursors. In the case of the bis(salicylaldiminato)copper(II) and -palladium(II) complexes

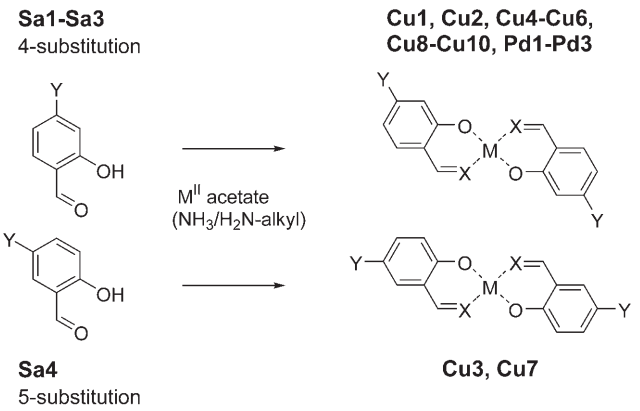

Scheme 1. Synthesis of the functionalised bis(salicylaldiminato)/bis(aldehydato)M^{II} complexes: M = Cu^{II}, Pd^{II}; X = O, NH, NR; Y = OR (4- or 5-position); R, R′ = *n*-alkyl (Table 1);[36] salicylaldehyde-derived ligands: **Sa1**: Y = OC_8H_{17}; **Sa2**: Y = $OC_{12}H_{25}$; **Sa3**: Y = $OC_{16}H_{33}$; **Sa4**: Y = $OC_{12}H_{25}$.

Table 1. Substitution pattern of the M^{II} complexes classified by ligand types.

Complex		Metal	X	Y[a]
aldehyde complexes	**Cu1**	Cu^{II}	O	4-OC_8H_{17}
C=O	**Cu2**	Cu^{II}	O	4-$OC_{12}H_{25}$
	Cu3	Cu^{II}	O	5-$OC_{12}H_{25}$
	Pd1	Pd^{II}	O	4-$OC_{12}H_{25}$
	Pd2	Pd^{II}	O	4-$OC_{16}H_{33}$
aldimine complexes	**Cu4**	Cu^{II}	NH	4-OC_8H_{17}
C=NH	**Cu5**	Cu^{II}	NH	4-$OC_{12}H_{25}$
	Cu6	Cu^{II}	NH	4-$OC_{16}H_{33}$
	Cu7	Cu^{II}	NH	5-$OC_{12}H_{25}$
	Pd3	Pd^{II}	NH	4-$OC_{12}H_{25}$
aldimine complexes	**Cu8**	Cu^{II}	NC_8H_{17}	4-$OC_{12}H_{25}$
C=NR	**Cu9**	Cu^{II}	NC_8H_{17}	4-$OC_{16}H_{33}$
	Cu10	Cu^{II}	$NC_{12}H_{25}$	4-$OC_{16}H_{33}$

[a] 4 and 5 indicate the position of the alkoxy side group.

Cu3–Cu7, **Pd3** (NH) and **Cu8–Cu10** (*N*-alkyl), the reactions were carried out by complexation (M^{II} acetate precursors) of the free ligands **Sa** in situ in the presence of an excess of ammonia or an *n*-alkyl amine.[35]

STM visualisation of self-assembled nanopatterns

Pattern type 1: We have previously presented the lamellar 2D structures of the C_{12} O-substituted bis(salicylaldehydato)copper(II) complex **Cu2**.[30] The corresponding Pd^{II} complex, **Pd1**, forms a similar lamellar adlayer (monolayer) at the 1,2,4-trichlorobenzene (TCB)/HOPG interface.[37] We obtained highly resolved STM images that show the *trans* isomers of **Pd1**, which were identified by the pre-orientation of the alkyl O-substituents (Figure 1).

The images allow a detailed analysis of the 2D array, which reveals short metal–metal distances of approximately 6.7 ± 0.2 Å within the lamellae. The arrangement of the complex cores suggests attractive interactions of the carbonyl protons with both the phenolate and carbonyl oxygen atoms of adjacent complexes due to their spatial proximity. Applying typical geometric parameters to the 2D structure

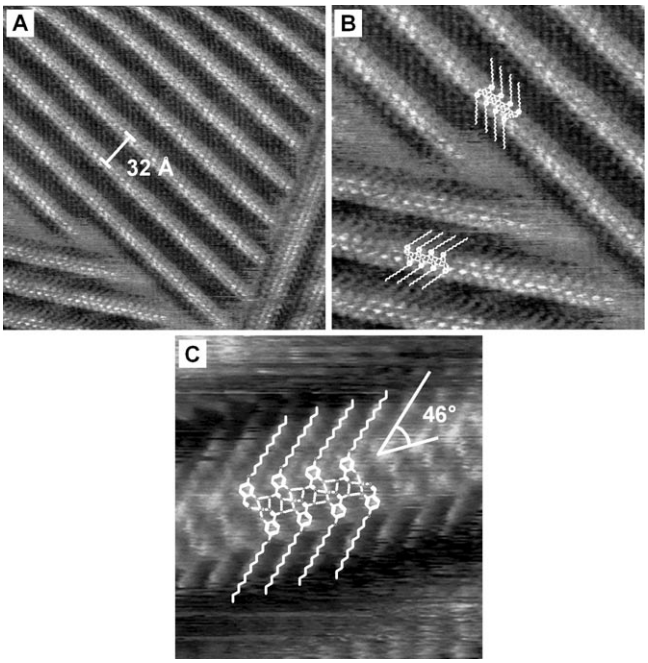

Figure 1. A) Wide-scan STM image showing the lamellar arrangement of **Pd1** from TCB solution. Image area: $28\times28\,nm^2$; $V_{set}=-0.31$ V, $I_{set}=19.6$ pA. B) Cut-out image of A, including superimposed models of the coexisting mirror images of the chiral 2D surface structures. C) Detailed high-resolution STM image of **Pd1** including superimposed structural formulae of the individual molecules. Image area: $6.0\times6.0\,nm^2$; $V_{set}=-0.71$ V, $I_{set}=20.5$ pA.

allowed us to evaluate the distances between these atoms to be about 2.6 ± 0.2 Å, which is in agreement with the typical lengths of weak inter- and intramolecular hydrogen bonds formed by aldehyde or aldimine protons with adjacent oxygen atoms (2.4–2.6 Å).[38–40] On the basis of these findings, we established a detailed model of the surface structure of **Pd1** that contains a network of weak hydrogen bonds, as depicted in Figure 2.

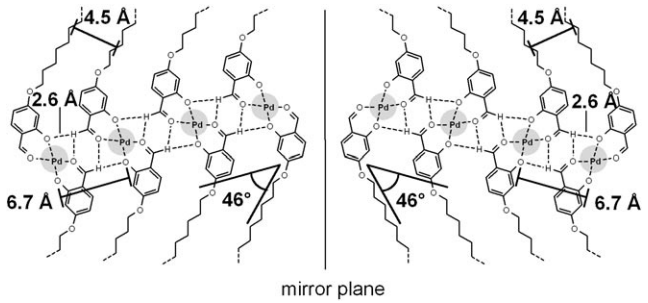

Figure 2. Proposed model for the molecular arrangement of **Pd1** within the two mirror forms of the chiral lamellar 2D patterns, including weak hydrogen bonds between adjacent complexes.

This model reveals that the highly ordered, lamellar 2D pattern of **Pd1** is chiral. The highly regular face-on deposition of the prochiral complexes onto the HOPG substrate results in loss of mirror-plane symmetry and produces two non-superimposable forms of enantiomeric surface species.[27] In the case of **Pd1**, as well as most of the other prochiral (C_{2h}-symmetric) *trans*-coordinated bis(salicylaldehydato) and bis(salicylaldiminato) complexes presented here, we observed the coexistence of homochiral, enantiomorphic domains that are statistically distributed over the whole HOPG surface.[41] Thus, on a macroscopic scale, the adlayers are achiral (no enantiomeric excess). The chiral domains are formed by the highly regular adsorption of the complexes from the same enantiotopic face, which can be attributed as either *Re* or *Si* relative to specific carbon atoms by employing the CIP convention for organic stereochemistry.[42] The 2D structure of **Pd1** presented in Figure 2, for example, corresponds to the *Si* adsorbate (adsorbed from the *Si* face) with respect to the alkoxy-substituted carbon atoms.[43] This terminology can be employed both for free ligands and metal complexes and is thus more convenient than an alternative description of the surface species relative to the metal ions, which are stereogenic centres as well (bridged, *trans*-coordinated heteroatoms). It is noteworthy that in the case of *cis*-coordinated complexes the face-on adsorption would result in the achiral, *meso* forms of the surface species (C_{2v} symmetry of the non-adsorbed complexes).

Comparison of the 2D order of the Pd^{II} complex **Pd1** with the corresponding Cu^{II} complex **Cu2** reveals slightly shorter metal–metal distances (6.7 ± 0.2 Å for **Pd1** versus 7.0 ± 0.2 in the case of **Cu2**). At the same time, the optimum periodicity of the densely packed alkyl chains (approximately 4.5 Å)[11] is maintained by a lower bending of the alkyl substituents of $46\pm2°$ with respect to the lamella axis (**Cu2**: $42\pm2°$). Consequently, these structural changes lead to an increased periodicity of the lamellae (34 ± 1 Å for **Pd1** versus 32 ± 1 Å for **Cu2**). These structural differences between **Pd1** and **Cu2** might be induced by slightly different bond lengths and angles in the Pd^{II} and Cu^{II} complexes and the weakness of the hydrogen bonds, which enables a reorientation of the complex cores. Furthermore, the shift of the position of the alkoxy side-group from the 4-position in **Cu2** to the 5-position in **Cu3**, while keeping the length constant (C_{12}), yields 2D patterns with an increased periodicity (36 Å in **Cu3** (5-position; see Supporting Information) versus 32 Å in **Cu2** (4-position)).

In the case of the bis(salicylaldehydato)palladium(II) and -copper(II) complexes, the periodicities of the lamellae can be controlled by varying the length of the alkyl chains (Table 2). The C_{16} O-substituted Pd^{II} complex **Pd2**, for example, forms lamellae with an increased periodicity (43 Å for C_{16} (Figure 3) versus 34 Å for **Pd1** (C_{12})). It is noteworthy that compound **Pd2** forms smaller domains than the cor-

Table 2. Periodicities of the lamellae within the type 1 pattern.

Compound	**Cu1**	**Cu2**	**Pd1**	**Cu3**	**Sa2**	**Pd2**
side group[a]	4-C_8	4-C_{12}	4-C_{12}	5-C_{12}	4-C_{12}	4-C_{16}
periodicity [±1 Å]	27	32	34	36	36	43

[a] 4 and 5 indicate the position of the side group; C_n is the short form of OC_nH_{2n+1}.

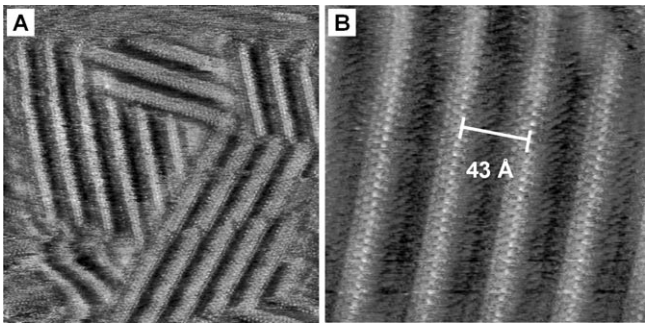

Figure 3. STM images of the self-assembled complex **Pd2** from TCB solution. A) Image area: 50×50 nm^2; $V_{set}=-570$ mV, $I_{set}=27.8$ pA. B) Image area: 19×19 nm^2; $V_{set}=-383$ mV, $I_{set}=27.8$ pA.

responding C_{12} O-substituted complex **Pd1**, presumably due to the faster adsorption of **Pd2**, which is caused by the stronger intermolecular van der Waals interactions between the longer C_{16} O-substituents.

In the case of the free salicylaldehydes **Sa** we did not observe any formation of 2D patterns directly from their solutions in TCB, hence it can be excluded that traces of free ligands were observed during the STM investigations of the metal complexes in this solvent. Surprisingly, a significantly slower 2D crystallisation of the free salicylaldehydes occurred when solutions in 1-octanol were employed. Fortunately, the resultant monolayers of **Sa2** were found to be stable enough to tolerate an exchange of the solvent (after evaporation of 1-octanol to dryness) for the less conductive 1,2,4-trichlorobenzene. This allowed us to achieve highly resolved STM images (Figure 4) that clearly show areas of the aromatic as well as aliphatic parts of the molecules. Similar to the corresponding metal complexes, a lamellar order is again observed, although with a slightly extended periodicity of the lamellae of 36 Å. The obtained surface structure (Figure 4B) shows a head-to-head arrangement of the ligands, which leads to a spatial proximity of the functional groups within the lamellae, as is observed for the corresponding metal complexes, where the ligands are linked through the metal ions.

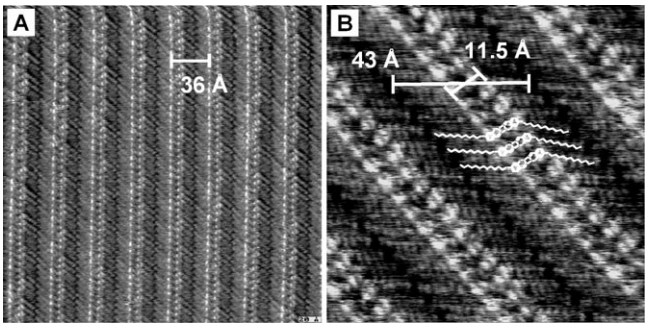

Figure 4. STM images of ligand **Sa2** from 1-octanol/TCB (see text) showing the lamellar order. A) Image area: 29×29 nm^2; $V_{set}=-131$ mV, $I_{set}=14.2$ pA. B) High-resolution image including superimposed chemical formulae and molecular parameters; image area: 10×10 nm^2; $V_{set}=-132$ mV, $I_{set}=14.2$ pA.

MacroModel calculations indicate the presence of hydrogen bonds between the carbonyl oxygen and the protons of two OH groups (Figure 5). The resultant planar dimers exhibit an extension of the aromatic cores of 11.5 Å and an alkyl end-to-end distance of approximately 43 Å, which agrees perfectly with the dimensions found in the STM images. The increased periodicity compared to the M^{II} complexes (**Sa2**: 36 Å; **Cu2:** 32 Å) at a similar angle of the alkyl substituents relative to the lamella axis (**Sa2**: $41\pm2°$ compared to $42\pm2°$ for compound **Cu2**) can be explained by the increased size of the dimer cores of the free ligands, as confirmed by comparison with the crystallographic data for the unsubstituted bis(salicylaldehydato)copper(II) complex.[36]

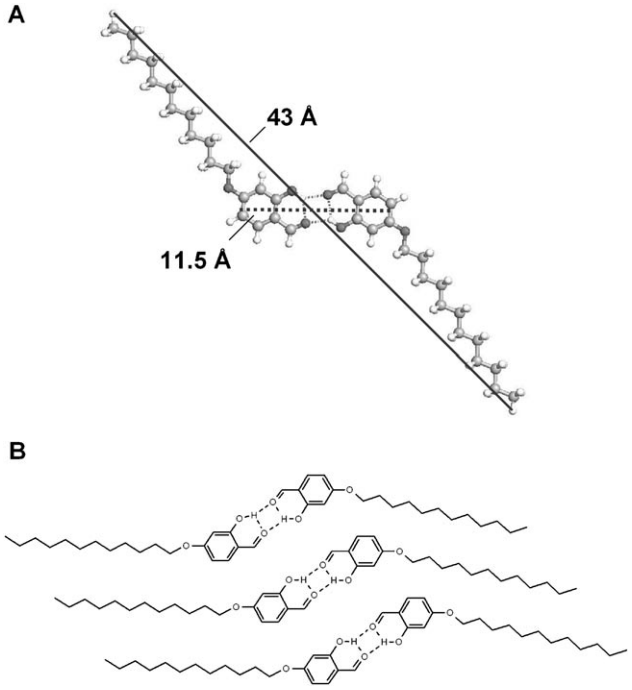

Figure 5. A) MacroModel (Amber) calculation of two C_{12} O-substituted salicylaldehyde molecules (**Sa2**) that are linked by hydrogen bonds into dimers. B) Model of the molecular order of **Sa2** at the liquid/HOPG interface.[44]

The highly ordered lamellar structures formed by the neutral alkoxy-substituted (4- and 5-position) bis(salicylaldehydato) complexes **Cu1**–**Cu3**, **Pd1** and **Pd2**, as well as the corresponding free salicylaldehyde (**Sa1**), at the solution/HOPG interface follow a general lamellar pattern which we call the homochiral *type 1 pattern* (Figure 6). Here, the periodicity of the lamellae depends mainly on the length of the alkoxy chains (Table 2), which stabilise the 2D structures by intermolecular van der Waals interactions within each lamella. Furthermore, we propose that weak hydrogen-bonding interactions promote the formation of this *type 1 pattern*. The resultant spatial proximities of the complex cores lead

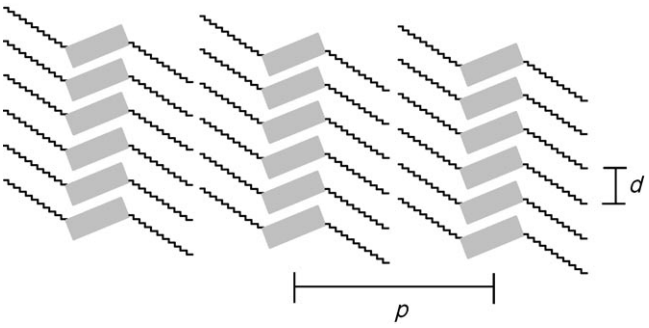

Figure 6. General model for the homochiral type 1 pattern[44] formed by free alkoxy-substituted salicylaldehydes as well as the corresponding M^{II} complexes **Sa1**, **Cu1**–**Cu3**, **Pd1** and **Pd2**; p: periodicity of the lamellae, d: relative metal–metal distance within the lamellae.

to short metal–metal distances of approximately 7 Å. Variation of the electronic structure (e.g. exchange of metal) or the substitution pattern affect the orientations of the complex cores or ligand dimers within the 2D structures only slightly. At the same time, the typical periodicity of densely packed alkyl chains of 4.5 Å[11] determines the degree of bending of the alkoxy substituents relative to the lamella axis (42–46°), which further influences the periodicity of the lamellae.

Type 2 pattern: Exchange of the aldehyde O-atom in the ligand molecules by the imine NH functionality leads to the corresponding bis(salicylaldiminato) complexes. The NH protons block the acceptor function (free electron pair) of the heteroatom, hence hydrogen bonding similar to that observed in the case of type 1 is now inhibited. Indeed, the three homologous Cu^{II}–imine complexes **Cu4**–**Cu6**, which bear alkyl substituents of different lengths (C_8, C_{12} and C_{16}, respectively) self-assemble at the liquid/HOPG interface with a different lamellar order (Figure 7) than the corresponding bis-salicylaldehydato complexes. They exhibit significantly increased distances between neighbouring complex cores and thus increased metal–metal distances (approximately 10 Å, versus about 7 Å for type 1). As a result of this structural expansion, the alkyl substituents from

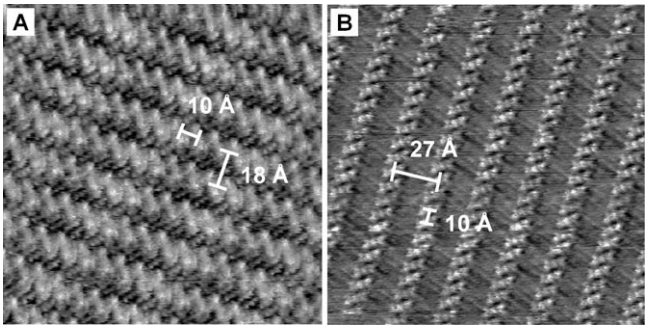

Figure 7. STM images of homologous alkoxy-substituted bis(salicylaldiminato)copper(II) complexes **Cu4** and **Cu6** from TCB solution. A) **Cu4**; image area: 15×15 nm^2; $V_{set}=-210$ mV, $I_{set}=28.4$ pA. B) **Cu6**; image area: 18×18 nm^2; $V_{set}=-0.53$ V, $I_{set}=25.4$ pA.

neighbouring lamellae interdigitate whilst maintaining the typical periodicity of 4.5 Å.[11] This results in decreased periodicities of the lamellae, which again depend on the length of the alkoxy substituents (18 Å for **Cu4** (C_8), 23 Å[30] for **Cu5** (C_{12}) and 27 Å for **Cu6** (C_{16}) versus the aldehyde complexes **Cu1** (C_8; 26 Å) and **Cu2** (C_{12}; 32 Å)).

Similar to the bis(salicylaldehydato) complexes, the exchange of Cu^{II} (**Cu5**, C_{12}) by Pd^{II} (**Pd3**, C_{12}) has no significant influence on the 2D assembly, which exhibits an equivalent periodicity of the lamellae (23 Å; see Supporting Information). The shift of the C_{12} O-substituent from the 4-position in **Cu5** to the 5-position in **Cu7** leads to a similar 2D ordering and packing density (Figure 8A; area per molecule

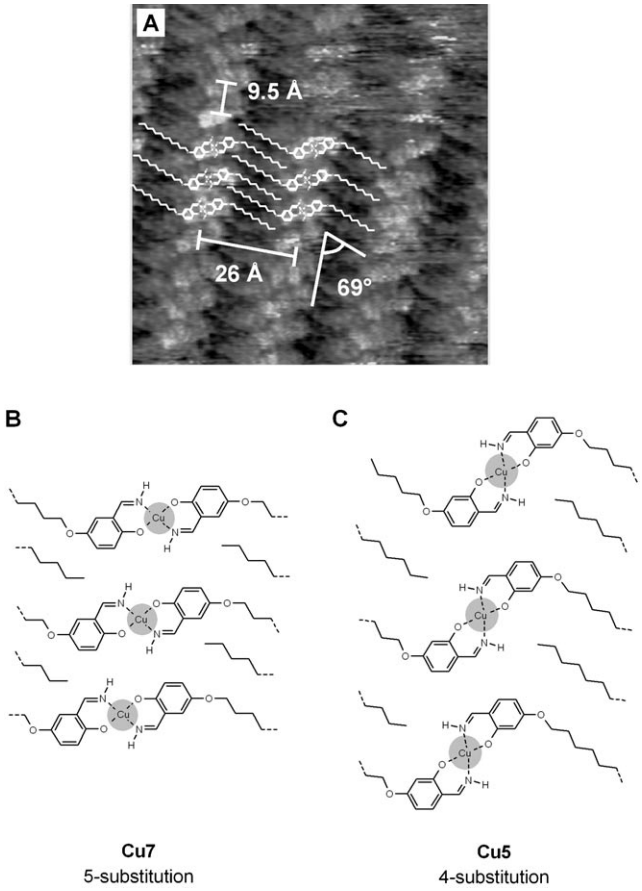

Figure 8. A) STM image of the adlayer of the 5-substituted (C_{12}) bis(salicylaldiminato)copper(II) complex **Cu7** from TCB solution, including superimposed structural formulae; image area: 10×10 nm^2; $V_{set}=-497$ mV, $I_{set}=30.8$ pA. B) Model of the molecular arrangement of the complex cores of **Cu7**.[44] C) Molecular arrangement of the complex cores of **Cu5**.[44]

for **Cu7** is 2.35 ± 0.1 nm^2 versus 2.30 ± 0.05 nm^2 for **Cu5**). However, the STM images reveal significantly changed relative orientations of the complex cores with respect to the lamella axis (Figures 8B and 8C). At the same time, slightly shorter relative metal–metal distances of approximately 9.5 Å are found (**Cu5**: 10 Å), which consequently lead to a larger angle between the alkyl chains and the lamella axis

(**Cu7**: 69±2°; **Cu5**: 60±2°). These two structural changes cause an increased periodicity of the lamellae (26 Å versus 23 Å in the case of **Cu5**).

On the basis of these findings, the observed lamellar 2D structures formed by the neutral, alkoxy-substituted bis-salicylaldiminato (NH) complexes **Cu4**–**Cu7** and **Pd3** can be generalised in a second densely packed, homochiral pattern (type 2; Figure 9). The main differences compared to type 1

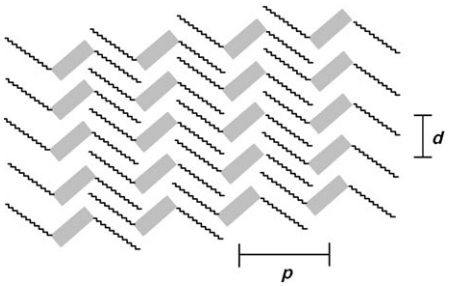

Figure 9. General model for the homochiral type 2 pattern,[44] formed by the bis(salicylaldiminato) (NH) M^{II} complexes **Cu4**–**Cu7** and **Pd3**; *p*: periodicity of the lamellae; *d*: relative metal–metal distance within the lamellae.

are the increased metal–metal distances of 9.5–10 Å and the interdigitation of the alkoxy substituents from adjacent lamellae. In effect, the periodicities of the lamellae are decreased and can be controlled stepwise by the varying the length of the alkoxy side groups (Table 3), as in the case of the bis(salicylaldehydato) complexes (Table 2).

Table 3. Compounds that form a type 2 pattern and the periodicities of their lamellae.

Complex	**Cu4**	**Cu5**	**Pd3**	**Cu7**	**Cu6**
side group[a]	4-C_8	4-C_{12}	4-C_{12}	5-C_{12}	4-C_{16}
periodicity [±1 Å]	19	23	23	26	27

[a] 4 and 5 indicate the position of the side group; C_n is the short form of OC_nH_{2n+1}.

Secondary 2D modification: In the case of **Cu5**, a secondary 2D modification can be found that is randomly distributed (Figure 10). Contrary to the primary structure (type 2 pattern), the adlayer is formed by an alternating deposition from the two enantiotopic faces of the C_{2h}-symmetric complex. The resultant 2D pattern consists of a racemic mixture of the two enantiomeric surface species (*Re*- and *Si*-adsorbate; Scheme 2) and exhibits longer metal–metal distances of approximately 12 Å. Comparison of the packing densities reveals a slightly increased area per molecule (2.4±0.05 nm^2 versus 2.3±0.05 nm^2 in the case of the type 1 pattern). In fact, the two different surface structures often coexist at the TCB/HOPG interface. However, the less dense packing along with a lower degree of overlap of the alkoxy substituents leads most probably to the predominance of the type 1 pattern over the secondary modification.

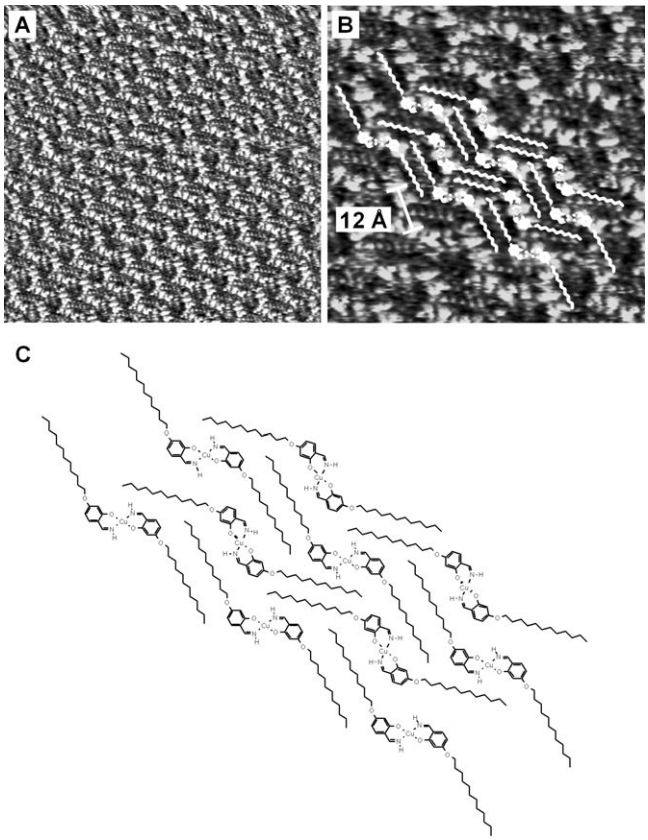

Figure 10. STM images of the secondary 2D modification of **Cu5** from TCB solution. A) image area: 20×20 nm^2; V_{set} = −257 mV, I_{set} = 31.8 pA. B) Cut-out image from image A, including superimposed structural formulae of **Cu5**; image area: 7×7 nm^2. C) Packing model of the secondary modification of **Cu5**, which consists of a highly ordered racemic mixture of enantiomeric *Re* and *Si* adsorbates.

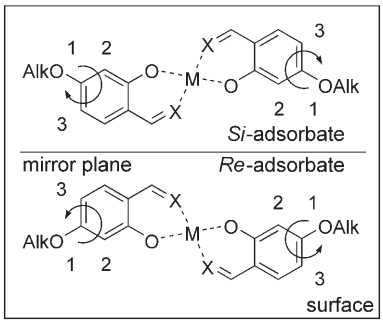

Scheme 2. Top view of the two enantiomeric surface species (*Re* and *Si* adsorbate with respect to the alkoxy-substituted carbon atoms).[43]

Type 3 pattern: To vary the molecular arrangement at the liquid/solid interface further, additional N-substituents were incorporated in the bis(salicylaldiminato) complexes. Previously, we have found that this functionalisation has a substantial impact on the order by suppressing the formation of lamellar structures completely and affording clearly separated complex "islands" of **Cu10** (Figure 11).[30] We established a reasonable model in which the *N*-alkyl substituents do not

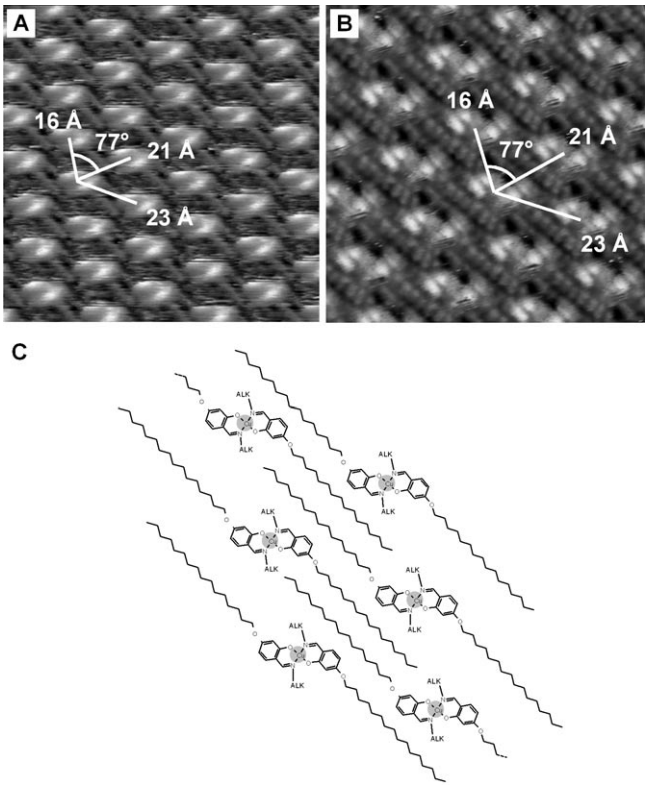

Figure 11. STM images of the adlayers of **Cu9** and **Cu10** from TCB solution, exhibiting partly resolved C_{16} *O*-alkyl substituents. A) **Cu10**: Image area: 10×10 nm^2; $V_{set}=-200$ mV, $I_{set}=21.6$ pA. B) **Cu9**: Image area: 6.5×6.5 nm^2; $V_{set}=-0.62$ V, $I_{set}=20.7$ pA. C) Model of the 2D pattern of **Cu9** and **Cu10**.

interact with the surface but point their tails into the solution, an effect which is known for other alkyl-substituted organic systems.[13,45,46] These assumptions[30] were confirmed by additional high-resolution STM images of the complex **Cu10** with different contrasts, which exhibit partly resolved alkyl chains that correspond to the relative orientation in the model (Figure 11 A).

The proposed model was further verified by a small series of related Cu^{II} complexes in which the lengths of the *O*- and *N*-alkyl chains were varied (**Cu8–Cu10**). In a first modification, the C_{12} N-substituents were replaced by shorter C_8 chains (**Cu9**) while the length of the alkoxy side-groups was kept constant (C_{16}). Here, we obtained high-resolution STM images in which the orientation of the alkyl groups as well as the complex cores are in accordance with the 2D structure formed by **Cu10** (Figure 11 B).[30] In effect, the 2D unit cells (area: 2.9 ± 0.05 nm^2; angle: $77\pm2°$), and thus the relative metal–metal distances (16 ± 1 Å, 21 ± 1 Å, 23 ± 1 Å), are equivalent.

In a second variation, the length of the *N*-alkyl chain was kept constant (C_8) while the length of the O-substituent was reduced from C_{16} (**Cu9**) to C_{12} (**Cu8**). This modification again afforded 2D "island" patterns, but with significantly decreased areas per molecule (2.5 ± 0.1 nm^2 for **Cu8** versus 2.9 ± 0.05 nm^2 in the case of **Cu9** and **Cu10**) and thus different relative metal–metal distances (Table 4). These findings revealed that the 2D order depends strongly on the length of the alkoxy side groups which, in turn, interact with the surface, whereas the length of the N-chains has no influence on the 2D patterning in the case of **Cu8–Cu10**.

Table 4. Structural parameters of the 2D patterns of **Cu8–Cu10**.

	Complex[a]		Metal–metal distances [±1 Å][b]			Area per molecule [±0.1 nm^2]
Cu8	OC_{12}	NC_8	16	16	20	2.5
Cu9	OC_{16}	NC_8	16	21	23	2.9
Cu10	OC_{16}	NC_{12}	16	21	23	2.9

[a] OC_n and NC_n are the short forms for OC_nH_{2n+1} and NC_nH_{2n+1}, respectively. [b] relative metal–metal distances A, B, and C, respectively (see Figure 12).

Comparison of the established model for **Cu10** with the 2D structure of **Cu6** (type 2 pattern, Figure 8 C) reveals a close relationship between the molecular arrangements of the NH- and *N*-alkyl-substituted bis-salicylaldiminato complexes, as demonstrated in Scheme 3. We assume that the sp^2-hybridised nitrogen atoms in **Cu10** (**Cu8**, **Cu9**) direct the attached CH_2 groups of the alkyl substituents into the complex plane. As a consequence, the increased steric demand next to the imine functionalities causes an expansion of the

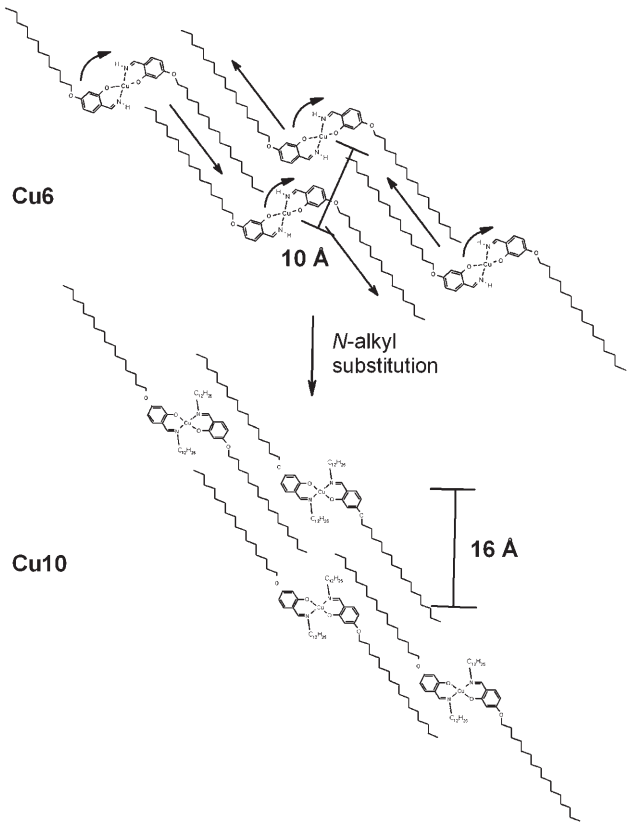

Scheme 3. Model of the 2D structure of **Cu10** emerging from the type 2 pattern (**Cu6**) by expansion of the 2D array along the C_{16} O-substituents.[44]

2D structure along the *O*-alkyl chains of adjacent complexes, combined with a slight reorientation of the complex cores.

On the basis of these results, we established a further modified homochiral (type 3) pattern that exhibits, in general, a distorted hexagonal order of the complexes and further increased relative metal–metal distances of approximately 16 Å (Figure 12). The additional N-substituents at the imine

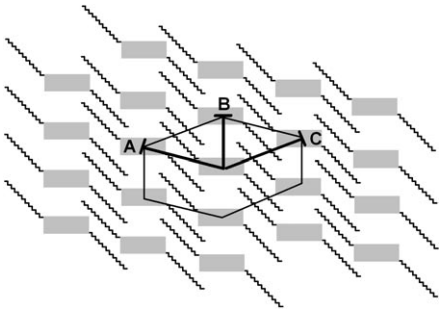

Figure 12. General model for the homochiral, distorted hexagonal type 3 pattern[44] formed by the bis(salicylaldiminato) (*N*-alkyl) M^{II} complexes **Cu8**–**Cu10**; A, B, C: relative metal–metal distances.

functionalities play a decisive role in this new pattern type by inducing significantly extended relative positions of the complex cores. However, the *N*-alkyl chains seem to interact only partly on the surface, pointing their tail into the solution, whereas the alkoxy side-groups mainly determine the structural parameters and thus the three characteristic relative metal–metal distances (A, B, C) of the 2D arrays.

Conclusion

We have shown that neutral alkyl/alkoxy-functionalised bis(salicylaldehydato)/bis(aldiminato)–M^{II} complexes can be successfully employed for 2D self-assembly at a liquid/solid interface. The relative ease of synthetic modification makes this class of metal complexes highly suitable for the nanopatterning of surfaces. The different functional aldehyde (C=O) and aldimine (NH, *N*-alkyl) groups lead to the formation of three related, but basically different, homochiral pattern types (Scheme 4), as well as a secondary 2D structure that consists of a racemic mixture of the two enantiomeric surface species. Bis(salicylaldehydato)M^{II} complexes form lamellar 2D structures with a spatial proximity of the complex cores due to the presence of a network of weak intermolecular hydrogen bonds. The corresponding bis-salicylaldiminato (NH) complexes form lamellae with increased relative metal–metal distances and shorter periodicities of the lamellae due to interdigitation of the alkyl chains. The incorporation of additional *N*-alkyl side groups leads to a further expansion of the 2D structure to afford "island" structures. Within the different 2D patterns, the relative metal–metal distance increases stepwise from 7 to 10 to 12 to 16 Å. Further changes of the chemical structures, such as variation of the metal ions or the position and length of the alkoxy side groups, allow an absolute fine-tuning of the relative metal–metal distances. The concepts presented here offer access to a large portfolio of further related 2D structures within the presented pattern types and can therefore be used as a highly effective tool for the nanodecoration of surfaces.

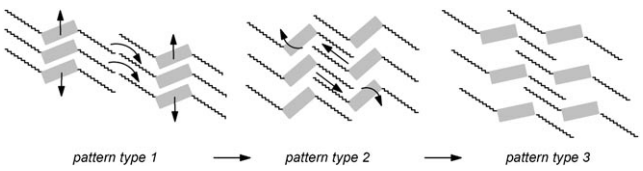

Scheme 4. Pattern types 1–3 emerging from each other.[44]

Our major long-term goal for such 2D nanopatterns is their application in catalysis, which means that catalytically interesting metal ions need to be employed. Studies in this direction are underway and need to be performed, in the case of air- or water-sensitive compounds, under an inert gas atmosphere. The major aim is the tailored variation of active sites in order to optimise spatial interactions and thus catalytic reactions. The chirality of the adlayers is particularly interesting for enantioselective processes. The key will be the transfer of additional chiral information into the adlayers, for example through chiral side groups, chiral solvents, or co-assembled chiral molecules, so that one of the two enantiomeric forms of the chiral 2D patterns is preferred.[29] Related dinuclear complexes will further extend the 2D patterns to shorter metal–metal distances, which might allow a direct cooperation of the metal ions and thus give access to important catalytic reactions for which more than one reactive centre is required.

Experimental Section

Materials and methods: All syntheses were performed by using standard laboratory equipment. Solvents and reagents were purchased from Aldrich, Fluka, Merck or Acros and used as received. Ammonia was employed as a solution in methanol (7 N, Acros). NMR spectra were recorded with a Bruker AMX400 spectrometer at 400 MHz (^{1}H) or 100 MHz (^{13}C), with $CDCl_3$ as solvent. Chemical shifts, δ, are given in ppm relative to the signal of $CDCl_3$ ($\delta_H = 7.24$ ppm, $\delta_C = 77.0$ ppm). IR spectra were obtained from KBr pellets with a Bruker IFS 113 V/IFS 66 V instrument. Elemental compositions (C, H, N) were determined on an Elementar Vario EL.

Synthesis of 2-hydroxy-4-(*n*-octyloxy)benzaldehyde (Sa1): 2,4-Dihydroxybenzaldehyde (4.00 g, 29.2 mmol), *n*-octyl bromide (5.64 g, 29.2 mmol) and $KHCO_3$ (2.93 g, 29.2 mmol) were stirred in DMF (100 mL) for 3 h under reflux. The mixture was then cooled to 0 °C and poured into an aqueous solution of hydrochloric acid (6 N, 100 mL). The mixture was extracted with dichloromethane and the combined organic layers were concentrated in vacuo and purified by column chromatography (silica; *n*-hexane/ethyl acetate, 9:1) to yield a colourless oil. Yield: 3.26 g (13.0 mmol, 45%); ^{1}H NMR ($CDCl_3$): $\delta = 0.86$ (t, $^3J = 6.9$ Hz, 3H; CH_3), 1.28 (m, 8H; CH_2), 1.40 (m, 2H; CH_2), 1.76 (q, $^3J = 7.1$ Hz, 2H; CH_2), 3.97 (t, $^3J = 6.6$ Hz, 2H; OCH_2), 6.38 (d, $^4J = 2.3$ Hz, 1H$_{arom}$), 6.49 (dd, $^3J = 8.6$ Hz, $^4J = 2.3$ Hz, 1H$_{arom}$), 7.38 (d, $^3J = 8.6$ Hz, 1H$_{arom}$), 9.67 (s, 1H;

CH=O), 11.46 (s, 1H; OH) ppm; ^{13}C NMR ($CDCl_3$): δ = 14.1, 22.6, 25.9, 28.9, 29.2, 31.74, 68.54, 101.0, 108.7, 115.0, 135.1, 164.5, 166.4, 194.3 ppm; elemental analysis calcd (%) for $C_{19}H_{30}O_3$: C 71.91, H 8.79; found: C 71.66, H 8.98.

Synthesis of 4-(*n*-dodecyloxy)-2-hydroxybenzaldehyde (Sa2): 2,4-Dihydroxybenzaldehyde (5.00 g, 36.2 mmol), *n*-dodecyl bromide (9.02 g, 36.2 mmol) and $KHCO_3$ (3.63 g, 36.2 mmol) were stirred in DMF (100 mL) for 3 h under reflux. The mixture was then left to cool to room temperature and poured into an aqueous solution of hydrochloric acid (6 N, 150 mL). The precipitate formed was filtered off and purified by column chromatography (silica; *n*-hexane/ethyl acetate, 9:1) to yield a white solid. Yield: 2.60 g (8.5 mmol, 23%); ^{1}H NMR ($CDCl_3$): δ = 0.86 (t, ^3J = 6.9 Hz, 3H; CH_3), 1.22–1.35 (m, 16H; CH_2), 1.39–1.46 (m, 2H; CH_2), 1.74–1.81 (m, 2H; CH_2), 3.98 (t, ^3J = 6.6 Hz, 2H; OCH_2), 6.39 (d, ^4J = 2.3 Hz, 1H$_{arom}$), 6.50 (dd, ^3J = 8.6 Hz, ^4J = 2.3 Hz, 1H$_{arom}$), 7.39 (d, ^3J = 8.6 Hz, 1H$_{arom}$), 9.68 (s, 1H; CH=O), 11.45 (s, 1H; OH) ppm; ^{13}C NMR ($CDCl_3$): δ = 14.1, 22.7, 25.9, 28.9, 29.3, 29.5–29.6, 31.9, 68.6, 101.1, 108.8, 115.0, 135.2, 164.6, 166.5, 194.3 ppm; elemental analysis calcd (%) for $C_{19}H_{30}O_3$: C 74.47, H 9.87; found: C 74.34, H 9.94.

Synthesis of 4-(*n*-hexadecyloxy)-2-hydroxybenzaldehyde (Sa3): The synthesis of **Sa3** was carried out as for **Sa2** but with 2,4-dihydroxybenzaldehyde (3.00 g, 21.7 mmol), *n*-hexadecyl bromide (6.63 g, 21.7 mmol) and $KHCO_3$ (2.17 g, 21.7 mmol) in DMF (75 mL). The reaction mixture was poured into an aqueous solution of hydrochloric acid (6 N, 100 mL) and separated by column chromatography (silica; *n*-hexane/ethyl acetate, 4:1). Yield: 2.35 g (6.5 mmol, 30%); ^{1}H NMR ($CDCl_3$): δ = 0.86 (t, ^3J = 6.9 Hz, 3H, CH_3), 1.20–1.35 (m, 24H; CH_2), 1.38–1.46 (m, 2H; CH_2), 1.73–1.80 (m, 2H; CH_2), 3.98 (t, ^3J = 6.6 Hz, 2H; OCH_2), 6.39 (d, ^4J = 2.0 Hz, 1H$_{arom}$), 6.50 (dd, ^3J = 8.6 Hz, ^4J = 2.0 Hz, 1H$_{arom}$), 7.39 (d, ^3J = 8.6 Hz, 1H$_{arom}$), 9.68 (s, 1H; CH=O), 11.46 (s, 1H; OH) ppm; ^{13}C NMR ($CDCl_3$): δ = 14.1, 22.7, 25.9, 28.9, 29.3, 29.4, 29.5, 29.6–29.7, 31.9, 68.6, 101.0, 108.8, 115.0, 135.2, 164.5, 166.5, 194.3 ppm; elemental analysis calcd (%) for $C_{23}H_{38}O_3$: C 76.20, H 10.56; found: C 76.02, H 10.49.

Synthesis of 5-(*n*-dodecyloxy)-2-hydroxybenzaldehyde (Sa4): A mixture of hydroquinone (20.10 g, 183 mmol), *n*-dodecyl bromide (34.50 g, 138 mmol) and NaOH (5.50 g, 138 mmol) in ethanol (150 mL) was vigorously stirred at reflux under argon for 6 h. The mixture was then left to cool to room temperature. The white precipitate formed was filtered off and identified as the bis(alkoxy) side product. Addition of H_2O to the supernatant led to the precipitation of the crude monoalkoxy product, which was filtered off. The solid was recrystallised from *n*-hexane, washed with water and dried in vacuo to yield white needles of 4-(*n*-dodecyloxy)phenol. Yield: 15.74 g (56.5 mmol, 41%); ^{1}H NMR ($CDCl_3$): δ = 0.86 (t, ^3J = 6.8 Hz, 3H; CH_3), 1.22–1.34 (m, 16H), 1.38–1.45 (m, 2H), 1.69–1.76 (m, 2H), 3.87 (t, ^3J = 6.6 Hz, 2H; OCH_2,), 4.40 (s, 1H; OH), 6.75 (m, 4H$_{arom}$) ppm; ^{13}C NMR ($CDCl_3$): δ = 14.1, 22.7, 26.0, 29.3, 29.4, 29.6–29.7, 31.9, 68.8, 115.6, 116.0, 149.3, 153.4 ppm.

4-(*n*-Dodecyloxy)phenol (2.00 g, 7.2 mmol) was then treated with hexamethylenetetramine (2.80 g, 20.0 mmol) in trifluoroacetic acid (10 mL). The suspension was vigorously stirred for 14 h at 100 °C and for a further 50 h at room temperature. At the end of this period an aqueous solution of hydrochloric acid (4 N, 10 mL) was added and the mixture extracted with CH_2Cl_2 and hexane. The combined organic layers were washed with an aqueous solution of hydrochloric acid (4 N), H_2O and a saturated aqueous solution of NaCl. The organic layer was concentrated in vacuo, and the obtained black oil was purified by column chromatography (silica; hexane/ethyl acetate, 9:1) to yield the yellow solid product. Yield: 0.40 g (1.3 mmol, 18%); ^{1}H NMR ($CDCl_3$): δ = 0.86 (t, ^3J = 6.8 Hz, 3H; CH_3), 1.22–1.35 (m, 16H; CH_2), 1.39–1.46 (m, 2H; CH_2), 1.72–1.79 (m, 2H; CH_2), 3.91 (t, ^3J = 6.6 Hz, 2H; OCH_2), 6.89 (d, ^3J = 9.1 Hz, 1H$_{arom}$), 6.97 (d, ^4J = 3.0 Hz, 1H$_{arom}$), 7.12 (dd, ^3J = 9.1 Hz, ^4J = 3.0 Hz, 1H$_{arom}$), 9.82 (s, 1H; CH=O), 10.62 (s, 1H; OH); ^{13}C NMR ($CDCl_3$): δ = 14.1, 22.7, 26.0, 29.2, 29.3, 29.4, 29.5–29.6, 31.9, 68.9, 116.1, 118.6, 120.0, 125.8, 152.2, 155.9, 196.1 ppm; IR (KBr): $\tilde{\nu}$ = 1671 cm^{-1} (C=O); elemental analysis calcd (%) for $C_{19}H_{30}O_3$: C 74.47, H 9.87; found: C 74.02, H 9.83.

Synthesis of complex Cu1: A solution of copper(II) acetate monohydrate (53.8 mg, 0.27 mmol) in a mixture of ethanol and water (1:1, 14 mL) was added to a solution of **Sa1** (135.5 mg, 0.54 mmol) in ethanol (5 mL). The mixture was stirred for 1 h under reflux and then left to cool to room temperature. A solid precipitated during the reaction, and this was filtered off, washed with ethanol and dried in vacuo to yield the pure green product. Yield: 133.9 mg (0.17 mmol, 64%); IR (KBr): $\tilde{\nu}$ = 1612 cm^{-1} (C=O); elemental analysis calcd (%) for $C_{30}H_{42}CuO_6$: C 64.09, H 7.53; found: C 64.34, H 7.51.

Synthesis of complex Cu2: The reaction was performed according to the methodology described for complex **Cu1** with solutions of copper(II) acetate monohydrate (64.1 mg, 0.32 mmol) in a mixture of ethanol and water (1:1, 6 mL) and **Sa2** (180.5 mg, 0.59 mmol) in ethanol (10 mL); 0.5 h reflux. Yield: 34.6 mg (0.05 mmol, 16%); IR (KBr): $\tilde{\nu}$ = 1626 cm^{-1} (C=O); elemental analysis calcd (%) for $C_{38}H_{58}CuO_6$: C 67.68, H 8.67; found: C 67.80, H 8.60.

Synthesis of complex Cu3: The reaction was performed according to the methodology described for complex **Cu1** with solutions of copper(II) acetate monohydrate (32 mg, 0.16 mmol) in ethanol (1.5 mL) and **Sa4** (103 mg, 0.34 mmol) in ethanol (1.5 mL). Yield: 72 mg (0.11 mmol, 67%); IR (KBr): $\tilde{\nu}$ = 1627 cm^{-1} (C=O); elemental analysis calcd (%) for $C_{38}H_{58}CuO_6$: C 67.68, H 8.67; found: C 67.68, H 8.64.

Synthesis of complex Pd1: A solution of palladium(II) acetate (65.6 mg, 0.29 mmol) in a mixture of ethanol and water (1:1, 6 mL) was added to a solution of **Sa2** (177.5 mg, 0.58 mmol) in ethanol (6.5 mL). The mixture was stirred for 1 h under reflux and then left to cool to room temperature. The solid precipitate formed was filtered off, washed thoroughly with H_2O and ethanol and dried in vacuo to yield the solid green product. Yield: 131.0 mg (0.18 mmol, 62%); ^{1}H NMR ($CDCl_3$) δ = 0.86 (t, ^3J = 6.9 Hz, 6H; CH_3), 1.18–1.48 (m, 36H; CH_2), 1.75 (m, 4H; CH_2), 3.93 (t, ^3J = 6.6 Hz, 4H; OCH_2), 6.27 (dd, ^3J = 8.8 Hz, ^4J = 2.3 Hz, 2H), 6.45 (d, ^4J = 2.3 Hz, 2H$_{arom}$), 7.21 (d, ^3J = 8.8 Hz, 2H$_{arom}$), 7.90 (s, 2H; CH=O) ppm; IR (KBr): $\tilde{\nu}$ = 1623 cm^{-1} (C=O); elemental analysis calcd (%) for $C_{38}H_{58}O_6Pd$: C 63.63, H 8.15; found: C 62.69, H 8.10.

Synthesis of complex Pd2: KOH (25.0 mg, 0.45 mmol) and palladium(II) acetate (46.0 mg, 0.20 mmol) were added to a solution of **Sa3** (153.0 mg, 0.42 mmol) in ethanol (7 mL). The mixture was stirred for 3 h under reflux and then left to cool to room temperature. The solid precipitate formed during the reaction was filtered off, washed thoroughly with H_2O and ethanol and dried in vacuo to yield the green product. Yield: 65.5 mg (0.08 mmol, 42%); ^{1}H NMR ($CDCl_3$) δ = 0.86 (t, ^3J = 6.9 Hz, 6H; CH_3), 1.18–1.48 (m, 52H; CH_2), 1.75 (m, 4H; CH_2), 3.93 (t, ^3J = 6.6 Hz, 4H; OCH_2), 6.27 (dd, ^3J = 8.8 Hz, ^4J = 2.3 Hz, 2H$_{arom}$), 6.45 (d, ^4J = 2.3 Hz, 2H$_{arom}$), 7.21 (d, ^3J = 8.8 Hz, 2H$_{arom}$), 7.90 (s, 2H; CH=O) ppm; IR (KBr): $\tilde{\nu}$ = 1623 cm^{-1} (C=O); elemental analysis calcd (%) for $C_{46}H_{74}O_6Pd$: C 66.61, H 8.99; found: C 66.86, H 9.10.

Synthesis of complex Cu4: A solution of **Sa1** (185 mg, 0.74 mmol) in a solution of ammonia in methanol (7 N, 7 mL) was stirred for 0.5 h under reflux. A solution of copper(II) acetate monohydrate (72 mg, 0.36 mmol) in ethanol (7 mL) was then added. The mixture was stirred for 0.5 h and then left to cool to room temperature. The precipitate formed was filtered off, washed with methanol and dried in vacuo to yield the green solid product. Yield: 129 mg (0.23 mmol, 64%); IR (KBr): $\tilde{\nu}$ = 1612 cm^{-1} (C=N); elemental analysis calcd (%) for $C_{30}H_{44}CuO_4N_2$: C 64.32, H 7.92, N 5.00; C 64.23, H 7.95, N 5.00.

Complexes **Cu5**–**Cu7** were synthesised according to the methodology described for complex **Cu4**.

Synthesis of complex Cu5: Synthesised from **Sa2** (150 mg, 0.49 mmol) in a solution of ammonia in methanol (7 N, 3 mL) and copper(II) acetate monohydrate (49 mg, 0.25 mmol) in a solution of ammonia in methanol (7 N, 1 mL). Yield: 90 mg (0.13 mmol, 55%); IR (KBr): $\tilde{\nu}$ = 1617 cm^{-1} (C=N); elemental analysis calcd (%) for $C_{38}H_{60}CuN_2O_4$: C 67.87, H 8.99, N 4.17; found: C 67.76, H 9.04, N 3.96.

Synthesis of complex Cu6: Synthesised from a solution of **Sa3** (163.93 mg, 0.45 mmol) in ethanol (7 mL) and copper(II) acetate monohydrate (47 mg, 0.24 mmol) in a solution of ammonia in methanol (7 N, 7 mL). Yield: 35.0 mg (0.04 mmol, 19%); IR (KBr): $\tilde{\nu}$ = 1616 cm^{-1} (C=N); elemental analysis calcd (%) for $C_{46}H_{76}CuO_4N_2$: C 70.41, H 9.76, N 3.57; found: C 70.61, H 9.70, N 3.53.

Synthesis of complex Cu7: Synthesised from **Sa4** (50 mg, 0.16 mmol) in a solution of ammonia in methanol (7 N, 20 mL) and copper(II) acetate monohydrate (16 mg, 0.08 mmol) in a solution of ammonia in methanol (7 N, 10 mL), 1 h reflux, washing with acetone. Yield: 20 mg (0.03 mmol, 38 %); elemental analysis calcd (%) for $C_{38}H_{60}CuO_4N_2$: C 67.87, H 8.99, N 4.17; found: C 67.32, H 8.94, N 4.29.

Synthesis of complex Pd3: A solution of **Sa2** (157.0 mg, 0.51 mmol) in ethanol (10 mL) was added to a solution of ammonia in methanol (7 N, 8 mL). The mixture was stirred for 0.5 h under reflux. A solution of palladium(II) acetate (57.2 mg, 0.26 mmol) in methanol (5 mL) was then added and the mixture stirred for 24 h at room temperature. At the end of this period, the precipitate formed was filtered off, washed with ethanol and dried in vacuo to yield the green-yellow solid product. Yield: 81.0 mg (0.11 mmol, 44 %); ^{1}H NMR ($CDCl_3$) $\delta = 0.86$ (t, $^3J = 6.8$ Hz, 6H; CH_3), 1.25 (m, 38H; CH_2), 1.75 (m, 4H; CH_2), 3.93 (t, $^3J = 6.6$ Hz, 4H; OCH_2), 6.24 (dd, $^3J = 8.6$ Hz, $^4J = 2.3$ Hz, $2H_{arom}$,), 6.41 (d, $^4J = 2.3$ Hz, $2H_{arom}$), 7.11 (d, $^3J = 8.6$ Hz, $2H_{arom}$), 7.75 (d, $^3J = 11.5$ Hz, 2H; CH=N), 7.90 (d, $^3J = 11.5$ Hz, 2H; NH) ppm; IR (KBr): $\tilde{\nu} = 1624$ cm^{-1} (C=N); elemental analysis calcd (%) for $C_{46}H_{74}O_6Pd$: C 63.81, H 8.45, N 3.92; found: C 64.16, H 8.41, N 3.82.

Synthesis of complex Cu8: Compound **Sa2** (354.3 mg, 1.16 mmol) and *n*-octylamine (149.4 mg, 1.16 mmol) were dissolved in ethanol (50 mL) and the mixture was stirred in the presence of a catalytic amount of acetic acid for 1 h under reflux. A solution of copper(II) acetate monohydrate (115.4 mg, 0.58 mmol) in a mixture of ethanol and water (1:1, 10 mL) was then added. The mixture was stirred for a further 0.5 h under reflux and then left to cool to room temperature. The solid precipitate formed was filtered off, washed with ethanol and dried in vacuo to yield a green solid product, which was recrystallised from a mixture of methanol and dichloromethane (1:1). Yield: 120.3 mg (0.13 mmol, 12 %); IR (KBr): $\tilde{\nu} = 1622$ cm^{-1} (C=N); elemental analysis calcd (%) for $C_{54}H_{92}CuO_4N_2$: C 72.25, H 10.26, N 3.12; found: C 71.93, H 10.11, N 3.14.

Synthesis of complex Cu9: The synthesis was carried according to the methodology given for complex **Cu8**, with **Sa3** (120.0 mg, 0.33 mmol), *n*-octylamine (0.05 mL, 0.30 mmol), a catalytic amount of acetic acid and a solution of copper(II) acetate monohydrate (100.0 mg, 0.50 mmol) in methanol (5 mL). Yield: 201.8 mg (0.20 mmol, 61 %); IR (KBr): $\tilde{\nu} = 1621$ cm^{-1} (C=N); elemental analysis calcd (%) for $C_{62}H_{108}CuO_4N_2$: C 73.80, H 10.79, N 2.78; found: C 73.44, H 10.64, N 2.70.

Synthesis of complex Cu10: The synthesis was carried according to the methodology presented for complex **Cu8**, with **Sa3** (168.7 mg, 0.47 mmol), *n*-dodecylamine (86.9 mg, 0.47 mmol) in ethanol (14 mL), a catalytic amount of acetic acid and a solution of copper(II) acetate monohydrate (47.7 mg, 0.24 mmol) in ethanol/H_2O (1:1, 7 mL). Yield: 211.9 mg (0.19 mmol, 78 %); IR (KBr): $\tilde{\nu} = 1620$ cm^{-1} (C=N); elemental analysis calcd (%) for $C_{70}H_{124}CuO_4N_2$: C 74.98, H 11.15, N 2.50; found: C 74.93, H 11.09, N 2.44.

STM: STM images were acquired in the constant-current (variable-height) mode under ambient conditions with the tip immersed in the supernatant solution. A low-current scanning tunnelling microscope (RHK Technology Inc., Troy, MI, USA; UHV 300, IVP 300, SPM 1000) was used with negative sample bias. STM tips were mechanically sharpened from Pt/Ir (90:10) wire. HOPG was used as substrate for the adlayers and at the same time for the internal calibration of the STM. Prior to imaging, the compounds to be investigated were dissolved in 1,2,4-trichlorobenzene or 1-octanol and a droplet of the saturated solution was placed on freshly cleaved HOPG. A physisorbed monolayer of each complex formed spontaneously at the liquid/HOPG interface. The brighter regions in the STM images correspond to ligand π-orbitals and related orbitals of the metal ions, whereas the interacting alkyl chains occur as darker areas. Distances and angles were measured over a wide range covering the largest possible number of molecules in order to reduce errors. The experiments were repeated several times with different tips in order to confirm the reproducibility of the highly ordered assemblies.

Acknowledgments

The authors thank the Deutsche Forschungsgemeinschaft (DFG) through the collaborative research centre "Sonderforschungsbereich" SFB 569 ("Hierarchic structure formation and function of organic–inorganic nanosystems") for financial support.

[1] U. Ziener, J.-M. Lehn, A. Mourran, M. Möller, *Chem. Eur. J.* **2002**, *8*, 951.
[2] Q. Xu, B. Zhang, L. Wan, C. Wang, C. Bai, X. D. Zhu, *Surf. Sci.* **2002**, *517*, 52.
[3] L. Scudiero, K. W. Hipps, D. E. Barlow, *J. Phys. Chem. B* **2003**, *107*, 2903.
[4] M. A. Lingenfelder, H. Spillmann, A. Dmitriev, S. Stepanow, N. Lin, J. V. Barth, K. Kern, *Chem. Eur. J.* **2004**, *10*, 1913.
[5] L. Scuderio, D. E. Barlow, K. W. Hipps, U. Mazur, *J. Phys. Chem. B* **2000**, *104*, 11899.
[6] K. Suto, S. Yoshimoto, K. Itaya, *J. Am. Chem. Soc.* **2003**, *125*, 14976.
[7] A. Zlatkin, S. Yudin, J. Simon, M. Hanack, H. Lehman, *Adv. Mater. Opt. Electr.* **1995**, *5*, 259.
[8] J. Foster, J. Frommer, *Nature* **1988**, *333*, 542.
[9] J. P. Rabe, S. Buchholz, *Science* **1991**, *253*, 424.
[10] D. M. Cyr, B. Venkataraman, G. W. Flynn, *Chem. Mater.* **1996**, *8*, 1600.
[11] C. L. Claypool, F. Faglioni, W. A. Goddard III, H. B. Gray, N. S. Lewis, R. A. Marcus, *J. Phys. Chem. B* **1997**, *101*, 5978.
[12] S. De Feyter, F. C. De Schryver, *J. Phys. Chem. B* **2005**, *109*, 4290.
[13] S. De Feyter, M. M. S. Abdel-Mottaleb, N. Schuurmans, B. J. V. Verkuijl, J. H. van Esch, B. L. Feringa, F. C. De Schryver, *Chem. Eur. J.* **2004**, *10*, 1124.
[14] M. M. S. Abdel-Mottaleb, N. Schuurmans, S. De Feyter, J. H. van Esch, B. L. Feringa, F. C. De Schryver, *Chem. Commun.* **2002**, 1894.
[15] P. Qian, H. Nanjo, N. Sanada, T. Yokohama, T. M. Suzuki, *Chem. Lett.* **2000**, 1118.
[16] X. Qiu, C. Wang, A. Q. Zeng, B. Xu, S. Yin, H. Wanf, S. Xu, C. Bai, *J. Am. Chem. Soc.* **2000**, *122*, 5550.
[17] T. Ohshiro, T. Ito, P. Bühlmann, Y. Umezawa, *Anal. Chem.* **2001**, *73*, 878.
[18] I. Sakata, K. Miyamura, *Chem. Commun.* **2003**, 156.
[19] Z. Wang, Q. Zeng, L. Wan, C. Wang, S. Yin, C. Bai, X. Wu, J. Yang, *Surf. Sci.* **2002**, *513*, L436.
[20] J. R. Gong, L. J. Wan, Q. H. Yuan, C. L. Bai, H. Jude, P. J. Stang, *Proc. Natl. Acad. Sci. USA* **2005**, *102*, 971.
[21] Y. Cai, S. L. Bernasek, *J. Phys. Chem. B* **2005**, *109*, 4514.
[22] V. Humblot, S. M. Barlow, R. Raval, *Prog. Surf. Sci.* **2004**, *34*, 1.
[23] A. M. Berg, D. L. Patrick, *Angew. Chem.* **2005**, *117*, 1855; *Angew. Chem. Int. Ed.* **2005**, *44*, 1821.
[24] Y. Wei, K. Kannappan, G. W. Flynn, M. B. Zimmt, *J. Am. Chem. Soc.* **2004**, *126*, 5318.
[25] F. Vidal, E. Delvigne, S. Stepanow, N. Lin, J. V. Barth, K. Kern, *J. Am. Chem. Soc.* **2005**, *127*, 10101.
[26] Z. Mu, Z. Wang, X. Zhang, K. Ye, Y. Wang, *J. Phys. Chem. B* **2004**, *108*, 19955.
[27] C. B. France, B. A. Parkinson, *J. Am. Chem. Soc.* **2003**, *125*, 12712.
[28] C.-J. Li, Q.-D. Zeng, C. Wang, L.-J. Wan, S.-L. Xu, C.-R. Wang, C.-L. Bai, *J. Phys. Chem. A* **2003**, *107*, 747.
[29] M. Parschau, S. Romer, K.-H. Ernst, *J. Am. Chem. Soc.* **2004**, *126*, 15398.
[30] P. Zell, F. Mögele, U. Ziener, B. Rieger, *Chem. Commun.* **2005**, 1294.
[31] K. Binnemans, Y. G. Galyametdinov, R. Deun, D. W. Bruce, S. R. Collinson, A. P. Polishchuk, I. Bikchantaev, W. Haase, A. V. Prosvirin, L. Tinchurina, I. Litvinov, A. Gubajdullin, A. Rakhmatullin, K. Uytterhoeven, L. van Meervelt, *J. Am. Chem. Soc.* **2000**, *122*, 4335.
[32] R. Paschke, S. Liebsch, C. Tschierske, M. A. Oakley, E. Sinn, *Inorg. Chem.* **2003**, *42*, 8230.
[33] Z. Wu, S. Wu, Y. Liang, *Spectrochim. Acta, Part A* **2003**, *59*, 1631.

[34] L. F. Lindoy, G. V. Meehan, N. Svenstrup, *Synthesis* **1998**, 1029.
[35] The in situ complexation of the NH imine complexes **Cu3**–**7** and **Pd3** was chosen because the free imine ligands could not be isolated as the pure compounds. In contrast, the isolation of the pure ligands was possible in the case of *N*-alkyl substitution (**Cu8**–**10**). The resultant metal complexes were identical with those obtained by in situ conversion.
[36] Unsubstituted or low substituted bis(salicylaldehydato)/bis(aldiminato)copper(II) complexes are typically square planar: a) E. N. Baker, D. Hall, T. N. Waters, *J. Chem. Soc. A* **1966**, 680; b) D. Hall, A. J. McKinnon, T. N. Waters, *J. Chem. Soc.* **1965**, 425; c) A. Elmali, Y. Elerman, *Z. Kristallogr.* **1995**, *210*, 612.
[37] At high concentrations we also observed areas with a different structure that seem to originate from the formation of double layers, with a different orientation of the lamellae within the two layers.
[38] P. Mal, U. Lourderaj, Parveen, P. Venugopalan, J. Narasimha Moorthy, N. Sathyamurthy, *J. Org. Chem.* **2003**, *68*, 3446.
[39] J. Lewiński, J. Zachara, P. Stolarzewicz, M. Dranka, E. KoŁodziejczyk, I. Justyniak, J. Lipkowski, *New J. Chem.* **2004**, *28*, 1320.
[40] G. R. Desiraju, *Chem. Commun.* **2005**, 2995.
[41] This is based on the high-resolution STM images that show the orientation of the alkyl chains. We did not observe any relationship between the chirality and the symmetry of the graphite substrate. However, a more detailed analysis of the surface structures reveals that the alkyl chains of neighbouring domains orient with typical angles of 0°, 60° and 120°. Due to the fact that the enantiomorphous domains coexist and the included angles between the lamellae and the alkyl-chain axes vary for each compound, the preferred orientations of the 2D arrays may differ from the above-mentioned angles.
[42] R. S. Cahn, C. K. Ingold, V. Prelog, *Angew. Chem.* **1966**, *78*, 413; *Angew. Chem. Int. Ed. Engl.* **1966**, *5*, 385.
[43] The top view of the *Si* adsorbate shows the *Re* face, and vice versa.
[44] The model represents one of the two enantiomeric forms of the chiral 2D patterns observed within the individual domains of the adlayers.
[45] C. B. Gorman, I. Touzov, R. Miller, *Langmuir* **1998**, *14*, 3052.
[46] Y. Kaneda, M. E. Stawasz, D. L. Sampson, B. A. Parkinson, *Langmuir* **2001**, *17*, 6185.

Received: August 15, 2005
Revised: December 19, 2005
Published online: March 7, 2006

